

# Ultraviolet variability in Solar-type members of the M67 open cluster

CARL MELIS<sup>1</sup> AND EKAMJOT KAIRE<sup>1</sup>

<sup>1</sup>*Department of Astronomy & Astrophysics, University of California San Diego, La Jolla, CA 92093-0424, USA*

## ABSTRACT

Solar-type members of the rich, nearly Solar-age and Solar-metallicity M67 open cluster are systematically investigated for ultraviolet variability. We utilize archival *Galaxy Evolution Explorer* (*GALEX*) data which features several imaging observation epochs spanning 5 years. Stars in or suspected of being in binary systems are avoided as well as stars that are blended in *GALEX* data, leading to a sample of 66 Solar-type stars. We assess variability over a variety of timescales that probe flares and longer-term trends that could be due to rotation and activity cycles. We do not find conclusive evidence for variability and determine that Solar-type members of M67 do not display  $>30\%$  near-ultraviolet variability over timescales ranging from days to years. Furthermore, within 50-second cadence lightcurves generated for each of the imaging epochs we find no near-ultraviolet flares that are  $\gtrsim 2\times$  the quiescent stellar near-ultraviolet emission level; the implied ultraviolet flare rate derived from this study is in mild tension with that derived for stars observed by *GALEX* in the primary *Kepler* field. This M67 *GALEX* study presents one of the most comprehensive ultraviolet datasets currently available for probing continuum emission variability for old Sun-like stars; the planned NASA UVEX mission has the potential to dramatically expand upon this work.

*Keywords:* G dwarf stars (556) — Stellar activity (1580) – Ultraviolet astronomy (1736)

## 1. INTRODUCTION

Stars are not static objects and experience phenomena ranging from dramatic and impulsive (flares; e.g., Kowalski 2024 and references therein) to subtle and predictable (rotation and magnetic cycles; e.g., Baliunas et al. 1995). With these events come changes in the overall luminous output from the star that can have different manifestations as a function of wavelength. While monitoring of the Sun has increasingly covered as many wavelengths as possible with as few temporal gaps as possible (e.g., Ayres 2020), monitoring efforts for other stars have been more sporadic in both temporal and wavelength coverage.

As of the writing of this article, the stellar and exoplanet communities are rallying to provide complete characterizations of the luminous output of late-type stars, especially within the ultraviolet domain (e.g., Wilson et al. 2025 and references therein). Absorption and scattering of stellar light by planetary atmospheres can significantly impact the structure, chemistry, and surface temperature of any orbiting planets (e.g., Krivova et al. 2009; Godolt et al. 2015; France et al. 2016; Airapetian et al. 2020 and references therein). These processes are strongly wavelength dependent and ultraviolet light like the bright H I Ly- $\alpha$  line plays a major role in driving the chemistry and heating of a planet’s middle atmospheric layers, especially through interactions with H<sub>2</sub>O, CH<sub>4</sub>, and CO<sub>2</sub>. Continuum

emission in the 1800-2400 Å range is an important driver for ozone production while wavelengths up to 3000 Å heat the middle atmosphere. When trying to identify Earth-like habitable planets, the interaction of any planet with the radiative energy provided by its host star are thus of decisive importance.

While active studies with missions like *TESS* and *JWST* will imminently inform on the atmospheres and habitability of planets in the habitable zone around late-type stars (e.g., Barkaoui et al. 2023; Madhusudhan et al. 2025), the future is slated to bring a facility capable of studying habitable zone Earth-like planets around Sun-like stars (e.g., Mamajek & Stapelfeldt 2024 and references therein). Through that lens we seek to examine the ultraviolet luminous output from Sun-like stars, particularly within the temporal domain. Such data has been extensively assessed for the Sun (e.g., Floyd et al. 2003; Krivova et al. 2006; Ayres 2020) and long-term monitoring suggests that while the Sun’s total (integrated over all wavelengths) irradiance changes by about 0.1% over a Solar cycle, its irradiance varies by a few percent between 2000-3000 Å, 10-20% between 1500-2000 Å, and more than 50% around the Ly- $\alpha$  emission line. A growing collection of studies are exploring the temporal domain of ultraviolet emission from other Sun-like stars with most focusing on line emission (e.g., Dravins et al. 1993b,a; Dorren & Guinan 1994; Metcalfe et al. 2007; Buccino & Mauas 2008; Ayres 2020, 2021; Kim et al. 2022; Kamgar et al. 2024) and some considering continuum variability (e.g., Sofia et al. 1989; Dorren & Guinan 1994; Buccino & Mauas 2008; Brasseur et al. 2019; Ayres 2020, 2021; Kim et al. 2022).

This paper attempts to determine the kind of ultraviolet irradiation environment that Solar-type stars can provide to any putative Earth-like planets that may orbit around them. We broadly seek to explore how hospitable Solar-type stars are to potentially habitable planets; such information will prove invaluable in future investigations of rocky planets around other Solar-type stars, especially as it pertains to assessing them for currently hosting life. Specifically, we seek to establish if other Solar-type stars follow the same general variability patterns as the Sun with a particular focus on continuum emission. Section 2 describes the target sample we have selected for this study, Section 3 shows the datasets used and how measurements are made from them, Section 4 presents our analysis approach and results, and Section 5 compares results from this study to the Sun and appropriate literature datasets with a brief reflection on how this study can be expanded.

## 2. TARGET SAMPLE

In this study we explore the ultraviolet variability patterns for Solar-type stars in the M67 open cluster ( $d=864$  pc; Noormohammadi et al. 2023). This sample selection is motivated by several factors. M67 has comparable age (e.g.,  $3.95^{+0.16}_{-0.15}$  Gyr; Reyes et al. 2024) and metallicity ( $[\text{Fe}/\text{H}]\approx+0.03$  dex; Casamiquela et al. 2019 and references therein) to the Sun which facilitates robust comparison to the Sun’s variability properties. *Gaia* data has resulted in a high-fidelity cluster membership list (e.g., Noormohammadi et al. 2023; Figure 1) featuring hundreds of Sun-like stars while spectroscopic monitoring studies (e.g., Lee et al. 2008; Smolinski et al. 2011; Pasquini et al. 2012; Geller et al. 2015; Brucalassi et al. 2017; Soubiran et al. 2018; Luo et al. 2019; Jönsson et al. 2020; Geller et al. 2021; Spina et al. 2021; Abdurro’uf et al. 2022; Randich et al. 2022; Rockosi et al. 2022; Hourihane et al. 2023) have revealed binary systems that could contaminate activity assessments. Of utmost importance for the present study is the availability of an ultraviolet dataset taken with the same instrument spanning a range of temporal scales (Section 3). The M67 ultraviolet study conducted herein provides the first ever look at the ultraviolet continuum variability levels for a large sample of well-characterized Solar-type stars having roughly Solar age and composition.

Past works have investigated the activity levels of Sun-like stars within M67. Giampapa et al. (2006) performed Ca II H+K activity analysis for 60 Sun-like stars in M67 and found that the range of

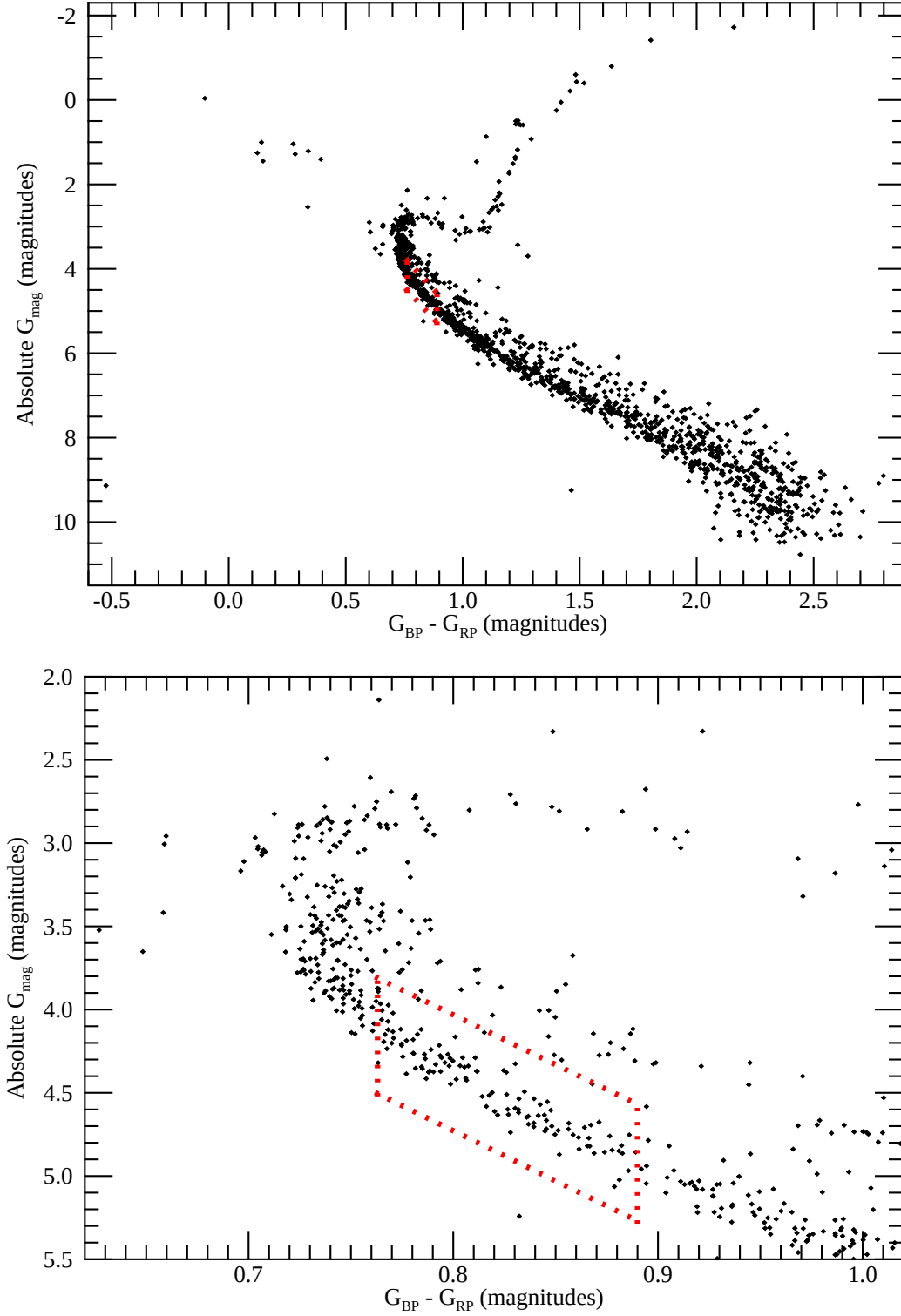


**Figure 1.** *Gaia* DR3 Hertzsprung-Russell diagram for M67 showing the Solar-type target selection; stars selected for this study are enclosed within the red dotted lines. No reddening corrections have been applied. The top panel shows all cluster members having membership probability  $>0.85$  as taken from [Noormohammadi et al. \(2023\)](#). The bottom panel zooms in on the Solar-type star region of the cluster. Error bars are omitted from the plots for the purposes of clarity.

activity levels observed included stars that were more active than the highest activity levels observed in the Sun. They also investigated long-term variability in Ca II H+K activity for their target stars, finding in general that the variability seen in Sun-like stars in M67 has higher amplitudes than that for the Sun over a comparable time range (Figure 9 from Giampapa et al. 2006). The reality of especially inactive stars found by Giampapa et al. (2006) was challenged by Curtis (2017) who explored the impact of interstellar medium (ISM) absorption in removing Ca II H+K flux. Curtis (2017) concludes that ISM absorption varies across the cluster and that any one cluster star may have more or less ISM absorption (especially from Ca II H+K) than another cluster star. Such external absorption would not explain variability behavior or especially active stars, however. Barnes et al. (2016) used *K2* data to derive rotational periods for 20 FGK stars in M67. Their analysis showed that the Sun appears rather normal in comparison to M67 Solar-like stars in terms of rotational properties, thus strengthening our comparison between them. Despite being covered by three different *K2* campaigns (497 30-minute cadence lightcurves for 234 stars across the 80-day duration campaigns 5, 16, and 18), Ilin et al. (2021) only find one candidate flare event in M67 (originating from a short-orbital period binary system as deduced from APOGEE data; Jönsson et al. 2020 and Abdurro’uf et al. 2022) suggesting luminous flare events are infrequent or possibly even absent within the cluster.

We draw our M67 target sample from Noormohammadi et al. (2023) and require prospective objects to have a membership probability  $>0.85$ . Target stars are selected from a narrow region of color-absolute magnitude space as shown in Figure 1. This region is used to obtain stars close to Solar-type, to avoid post-main sequence (including possibly early sub-giant) stars, and to ensure target stars are bright enough to be detected with reasonable significance ( $\gtrsim 10\sigma$ ) in at least one band by the *Galaxy Evolution Explorer* (*GALEX*) satellite (Section 3).

Further target vetting includes systematic searches for evidence of binarity in both *Gaia* and published radial velocity data. Candidates lying appreciably above the main cluster isochrone were excluded (Figure 1). Any target found to have a renormalized unit weight error (RUWE)  $\geq 1.1$  is flagged as potentially in a binary system as well as any star with detected radial velocity variability of any sort (we also exclude a few stars with no evidence for radial velocity variability but where the measured value was  $>5\sigma$  different from the cluster mean of  $+33.64 \text{ km s}^{-1}$ ; Geller et al. 2015). A final requirement is that target stars in the *GALEX* images of M67 must be sufficiently isolated to perform accurate photometry; each star was visually inspected in a *GALEX* near-ultraviolet (NUV) image and rejected if we could not construct a clean photometric extraction aperture and sky annulus (more details are in Section 3). Furthermore, any star not featured in more than one *GALEX* epoch was excluded from our analysis. Table 1 lists all target stars retained for photometric variability analysis.

### 3. *GALEX* PHOTOMETRY AND LIGHTCURVES

We utilized the multi-epoch visits to M67 by the *GALEX* satellite to conduct our investigation. *GALEX* was capable of obtaining near-ultraviolet (NUV;  $1771\text{--}2831 \text{ \AA}$ ,  $\lambda_{\text{eff}} 2315.7 \text{ \AA}$ ) and far-ultraviolet (FUV;  $1344\text{--}1786 \text{ \AA}$ ,  $\lambda_{\text{eff}} 1538.6 \text{ \AA}$ ) imaging over a  $\approx 1.2^\circ$  field-of-view (Morrissey et al. 2007). *GALEX* was demonstrated to have photometric repeatability between visits of 0.03 magnitudes in the NUV and 0.05 magnitudes in the FUV (Morrissey et al. 2007); these values should be viewed as noise floors for each filter. Table 2 lists all epochs used; any collection of visits spanning  $<10$  hours are treated as a single epoch. Not all epochs covered every star in the sample and some epochs were taken when the FUV channel was not operating. Magnitudes reported from *GALEX* are in the AB magnitude system (*Gaia* magnitudes are in the Vega system).

**Table 1.** M67 Solar-type Targets

ID	J2016 RA/DEC (sexagesimal)	J2016 RA/DEC (degrees)	$\pi$ (mas)	$G_{\text{mag}}$ (mag)	$M_G$ (mag)	$G_{\text{BP}} - G_{\text{RP}}$ (mag)	RUWE	$P_{\text{memb}}$
1	08 51 58.06 +12 00 59.59	132.9919027 +12.01655387	1.124	13.638	3.892	0.763	0.959	0.998
2	08 54 02.68 +12 08 04.20	133.5111697 +12.1345012	1.139	13.682	3.965	0.764	0.957	0.978
3	08 50 57.19 +12 05 36.41	132.7382901 +12.09344655	1.116	13.821	4.060	0.765	0.977	0.999
4	08 52 09.60 +11 46 46.19	133.0400139 +11.77949795	1.176	13.884	4.235	0.767	0.946	0.999
5	08 53 21.72 +11 17 14.62	133.3405192 +11.2873942	1.150	13.767	4.070	0.768	1.027	0.986
6	08 50 09.93 +11 59 53.91	132.5413914 +11.99830746	1.170	13.780	4.120	0.768	1.019	0.999
7	08 50 40.47 +11 42 11.53	132.6686445 +11.70320336	1.145	13.908	4.201	0.769	1.011	0.998
8	08 51 53.18 +12 03 31.98	132.9715656 +12.0588830	1.129	13.758	4.021	0.770	1.035	0.997
9	08 51 56.53 +11 48 12.49	132.9855281 +11.80346966	1.178	13.816	4.171	0.770	1.056	0.999
10	08 51 48.45 +11 42 22.86	132.9518937 +11.70635008	1.159	13.885	4.206	0.774	1.039	0.939
11	08 51 12.31 +11 18 38.72	132.8012981 +11.31075419	1.151	13.909	4.215	0.774	0.982	0.996
12	08 50 18.67 +12 16 01.00	132.577804 +12.26694538	1.146	13.986	4.283	0.775	1.074	0.997
13	08 51 38.73 +11 42 37.36	132.9113613 +11.71037788	1.100	13.978	4.185	0.777	0.975	0.999
14	08 53 40.02 +12 05 01.43	133.4167436 +12.0837308	1.125	13.923	4.180	0.780	0.953	0.992
15	08 51 15.04 +11 49 21.09	132.8126575 +11.8225261	1.136	13.987	4.264	0.780	1.014	0.999
16	08 50 38.66 +11 12 12.84	132.6610991 +11.20356562	1.120	14.015	4.261	0.780	0.971	0.998
17	08 50 56.51 +11 38 08.17	132.7354783 +11.63560363	1.186	13.981	4.352	0.781	0.979	0.999
18	08 53 34.71 +11 41 58.50	133.3946156 +11.6995826	1.135	13.662	3.938	0.782	0.987	0.995
19	08 52 30.26 +11 42 50.42	133.1261032 +11.71400676	1.068	13.976	4.119	0.784	0.988	0.997
20	08 51 18.71 +11 55 49.68	132.8279619 +11.9304678	1.142	13.979	4.268	0.785	1.018	0.999
21	08 50 56.31 +11 51 29.24	132.7346429 +11.85812287	1.167	13.959	4.295	0.786	0.972	0.997
22	08 50 11.60 +12 14 33.62	132.5483503 +12.24267153	1.166	14.034	4.367	0.788	0.935	0.994
23	08 50 00.83 +11 42 09.79	132.5034644 +11.70271836	1.176	14.022	4.374	0.790	1.004	0.997
24	08 50 48.10 +11 54 47.66	132.7004148 +11.91323806	1.128	13.952	4.214	0.793	0.974	0.999
25	08 50 22.79 +12 13 37.12	132.5949661 +12.22697823	1.114	14.041	4.276	0.793	0.983	0.997
26	08 52 11.38 +11 40 32.04	133.0474329 +11.67556711	1.147	14.074	4.371	0.793	1.020	0.998
27	08 52 09.93 +12 10 31.05	133.0413877 +12.1752927	1.141	14.002	4.289	0.794	0.891	0.998
28	08 51 34.11 +11 46 55.74	132.892119 +11.78215118	1.143	14.028	4.318	0.795	0.935	0.998
29	08 51 23.13 +11 54 04.98	132.8463869 +11.90138407	1.162	14.013	4.338	0.798	0.971	0.999
30	08 51 12.28 +11 54 22.96	132.8011626 +11.90637877	1.166	14.004	4.337	0.803	0.966	0.999
31	08 51 27.48 +11 53 02.43	132.8645079 +11.88400937	1.162	14.019	4.345	0.805	0.970	0.999
32	08 50 28.04 +11 54 50.54	132.6168447 +11.91403833	1.174	14.022	4.370	0.811	0.932	0.857
33	08 52 01.55 +12 03 54.19	133.0064639 +12.06505174	1.159	14.051	4.371	0.811	1.003	0.996
34	08 51 56.57 +11 47 24.96	132.985721 +11.79026558	1.148	14.223	4.522	0.814	1.055	0.998
35	08 51 55.14 +11 39 40.16	132.9797563 +11.66115531	1.152	14.207	4.515	0.817	1.010	0.999
36	08 51 14.33 +11 41 09.18	132.8096959 +11.68588288	1.139	14.329	4.611	0.820	0.969	0.999
37	08 50 09.58 +11 38 41.91	132.5399361 +11.64497559	1.148	14.332	4.632	0.821	1.008	0.997
38	08 51 20.03 +11 51 01.65	132.8334417 +11.85045922	1.112	14.146	4.377	0.825	1.012	0.998

**Table 1** continued on next page

**Table 1** (*continued*)

ID	J2016 RA/DEC (sexagesimal)	J2016 RA/DEC (degrees)	$\pi$ (mas)	$G_{\text{mag}}$ (mag)	$M_G$ (mag)	$G_{\text{BP}}-G_{\text{RP}}$ (mag)	RUWE	$P_{\text{memb}}$
39	08 51 36.02 +12 23 47.11	132.9001008 +12.39641961	1.150	14.206	4.509	0.826	0.928	0.987
40	08 50 21.56 +11 50 23.12	132.5898482 +11.83975787	1.141	14.345	4.630	0.826	1.084	0.998
41	08 50 58.33 +11 58 14.79	132.7430592 +11.97077596	1.124	14.337	4.592	0.830	0.998	0.984
42	08 51 53.88 +11 39 04.81	132.9744811 +11.65133687	1.132	14.349	4.619	0.831	0.949	0.999
43	08 52 00.40 +11 56 07.01	133.0016787 +11.93527943	1.169	14.196	4.536	0.832	0.937	0.999
44	08 51 12.52 +12 11 17.30	132.8021731 +12.18814015	1.132	14.222	4.492	0.834	0.985	0.998
45	08 51 48.93 +11 48 02.16	132.953887 +11.80060118	1.175	14.330	4.680	0.839	1.006	0.999
46	08 52 15.44 +11 53 01.46	133.0643474 +11.8837387	1.182	14.340	4.703	0.839	1.000	0.998
47	08 51 12.97 +11 57 00.88	132.8040507 +11.95024464	1.176	14.285	4.636	0.841	0.988	0.998
48	08 51 27.95 +11 50 11.87	132.8663975 +11.83663088	1.168	14.234	4.571	0.842	1.063	0.999
49	08 51 09.13 +11 57 00.31	132.7880497 +11.95008719	1.118	14.391	4.632	0.844	0.933	0.998
50	08 51 34.49 +11 43 49.44	132.8936995 +11.73040139	1.154	14.419	4.730	0.844	1.013	0.999
51	08 51 23.86 +11 38 52.11	132.8494072 +11.64780855	1.173	14.370	4.716	0.845	0.947	0.999
52	08 49 36.68 +12 30 53.41	132.4028389 +12.51483483	1.107	14.445	4.665	0.845	0.979	0.962
53	08 54 10.58 +12 16 37.62	133.5440834 +12.277117990	1.132	14.499	4.767	0.861	1.036	0.930
54	08 51 30.08 +11 27 31.50	132.8753246 +11.458749	1.153	14.441	4.750	0.849	0.974	0.998
55	08 52 45.49 +11 54 45.70	133.1895473 +11.91269295	1.133	14.454	4.726	0.851	0.930	0.998
56	08 50 52.29 +11 45 03.55	132.7178854 +11.75098493	1.205	14.465	4.870	0.851	0.979	0.999
57	08 51 01.46 +12 28 45.30	132.7560722 +12.479248025	1.171	14.496	4.838	0.861	1.091	0.979
58	08 51 35.46 +11 34 32.12	132.8977629 +11.57558909	1.161	14.496	4.819	0.865	0.984	0.998
59	08 53 12.28 +11 40 28.43	133.3011769 +11.67456306	1.181	14.501	4.862	0.868	1.007	0.996
60	08 51 30.74 +12 04 16.03	132.878095 +12.07112058	1.109	14.535	4.759	0.876	0.992	0.998
61	08 52 47.65 +11 57 26.16	133.1985207 +11.95726601	1.103	14.631	4.844	0.877	0.953	0.998
62	08 51 09.28 +11 33 32.98	132.7886738 +11.55915992	1.223	14.627	5.063	0.878	1.008	0.999
63	08 51 07.94 +11 58 53.32	132.7830938 +11.98147888	1.136	14.572	4.849	0.880	1.064	0.997
64	08 51 59.00 +11 41 49.16	132.9958397 +11.69698846	1.244	14.549	5.022	0.881	0.964	0.999
65	08 51 15.83 +11 40 30.28	132.8159657 +11.6750777	1.122	14.613	4.864	0.882	1.012	0.999
66	08 50 18.38 +11 54 23.98	132.5765685 +11.90666029	1.174	14.620	4.968	0.885	0.987	0.976

NOTE—RA/DEC,  $\pi$ , apparent magnitudes ( $G_{\text{mag}}$ ,  $G_{\text{BP}}-G_{\text{RP}}$ ) and RUWE come from *Gaia* DR3 (Gaia Collaboration et al. 2023). Uncertainties on  $\pi$  are generally 0.02 mas ( $\sim 2\%$ ), but may be larger if astrometric excess noise is present (this is only the case for a few stars in the sample and never exceeds 0.05 mas). Photometric errors are  $<1\%$ .  $M_G$  is calculated from the reported  $\pi$  and  $G_{\text{mag}}$ .  $P_{\text{memb}}$  is the membership probability as assessed by Noormohammadi et al. (2023).

To generate photometric measurements in the NUV and FUV (when present), we employ the gPhoton package (Million et al. 2016). Table 2 lists start and end times and durations for each epoch. Values are listed in *GALEX* time which is 315964800 seconds less than UNIX time (e.g., Million et al. 2016); for reference, a UNIX time of 1204545600.0 seconds (a *GALEX* time of 888580800.0 seconds) corresponds to 12:00 UT 03 March 2008. Start and end times as reported in Table 2 are designed to encompass all possible times when *GALEX* may have been recording photons for any given M67 star during a pointing toward the general direction of the cluster. We did not adjust the default



**gPhoton** edge limit that effectively truncates the *GALEX* field-of-view to  $\approx 1.1^\circ$ . Table 2 start and end times are fed directly into the **gPhoton gAperture** module when producing epochal photometry. Epoch start and end times are derived by examining the range of start (end) times for all stars in any given epoch as returned from the **gPhoton gFind** module, taking the earliest (latest) value, and padding it with  $-2000$  ( $+2000$ ) seconds. The epoch duration listed in Table 2 is calculated for this full range. The Total Exposure column of Table 2 gives a closer accounting of the actual amount of exposure time any star may have accrued during each epoch.

Each target is individually inspected in a *GALEX* image of M67 to determine the optimal aperture and background annulus radii to use for photometric extraction in all epochs; background count levels are assessed for each individual epoch. Generally, a radius of  $12.8''$  and annulus spanning  $16.0$ - $22.0''$  are used; roughly 20% of the targets benefited from truncated values of  $9.0''$  and  $12.8$ - $18.8''$  respectively when there was potential for contamination by nearby sources. Aperture sizes are chosen to ensure source photometry can be reliably compared across all epochs regardless of where the source fell in the *GALEX* field-of-view in any individual epoch (*GALEX* featured a significantly position-dependent point-spread function; Morrissey et al. 2007). **gAperture** is called with source positions as given in Table 1, radius and background annulus values as reported in Table 3, each epoch time range listed in Table 2, and directed to produce a single integrated magnitude and associated uncertainty for the band of interest (NUV and FUV are run separately). Table 3 reports for each source aperture corrections as suggested in Figure 4 of Morrissey et al. (2007) and measured epochal NUV photometry. Figure 2 plots absolute NUV magnitudes versus *Gaia* colors for all Table 1 targets.

After careful consideration of epochal FUV results, it was determined that most individual epochs did not actually result in a detection. Indeed, many of them reported either negative flux values or flux values smaller than (or certainly  $< 2\times$ ) the reported flux uncertainty. We conclude that *GALEX* was not sensitive enough to provide epochal FUV detections for M67 Sun-like stars. However, for the sake of completeness, we ran the **gAperture** module for each source covering all time ranges (encompassing the Epoch 1 start time to the Epoch 12 end time) to produce an all-epoch integrated FUV magnitude. Even in this situation, with most sources accruing  $\approx 7,000$  seconds of total FUV exposure time, many sources still produced non-detections. We converted non-detections to limits by taking  $2.5\times$  the flux uncertainty as the limiting flux and converting it to an FUV magnitude (any source with flux  $\geq 2.5\times$  the flux uncertainty was considered a detection). Table 3 reports FUV all-epoch integrated magnitudes or limits and Figure 2 plots the recovered values (including limits) as a function of target star *Gaia* color.

Lightcurves are generated with the same **gAperture** command used to produce epochal photometry for each target with a revised time range that encompassed the Epoch 1 start time to the Epoch 12 end time. An additional parameter specified the output as photometry for time bins of 50 seconds throughout the input time range; this cadence was motivated by comparison with Brasseur et al. (2019) as described in detail in Section 5. Given the inability to detect sources in epochal FUV photometry as described above, lightcurves are only generated for NUV data.

#### 4. ANALYSIS AND RESULTS

Being wary of the potential for varying interstellar medium levels between stars within M67 (see Curtis 2017 and references therein), we choose to initially focus our analysis at an intra-object level. Epochal measurements are assessed for each source, examining the difference between magnitudes measured in any given pair of epochs without repeating any epoch pairs (i.e., Epoch 1 – Epoch 2 excludes Epoch 2 – Epoch 1; the absolute value of each difference is taken to remove any effects

**Table 2.** *GALEX* M67 Epochs

Epoch	UT Date	MJD	Epoch Start	Epoch End	Epoch Duration	Total Exposure
		(days)	( <i>GALEX</i> time, sec)	( <i>GALEX</i> time, sec)	(hrs)	Time (sec)
1	2005-01-30	53400.58	791123761.995	791133774.995	2.8	95 + 96
2	2005-02-18	53419.59	792768195.995	792773889.995	1.6	1694
3	2006-01-21	53756.35	821838478.995	821873536.995	9.8	74 + 1313 + 1458
4	2006-01-23	53758.38	822039744.995	822045111.995	1.5	1367
5	2006-01-31	53766.73	822761930.995	822767294.995	1.5	1364
6	2006-02-15	53781.72	824057421.995	824061531.995	1.2	110
7	2008-01-28	54493.47	885552777.995	885556885.995	1.2	108
8	2008-03-01	54526.69	888422119.995	888427600.995	1.6	1481
9	2009-01-03	54834.48	915015145.995	915019708.995	1.3	183
10	2009-01-27	54858.85	917121681.995	917125955.995	1.2	274
11	2010-01-12	55208.24	947308128.995	947313806.995	1.6	1678
12	2010-01-13	55209.20	947390910.995	947396613.995	1.6	1703

NOTE—See Section 3 for a description of start, end, and duration times. Total Exposure Time gives the *GALEX*-reported on-sky time for all pointings conducted within a given epoch and doesn't account for detector dead time or shuttered time (see Million et al. 2016, 2023 and references therein); when multiple values appear, this means individual exposures separated by some gap are present within the reported epoch duration. MJD is the median Modified Julian Date value for all sources with data in a given epoch (individual values are reported in Table 3).

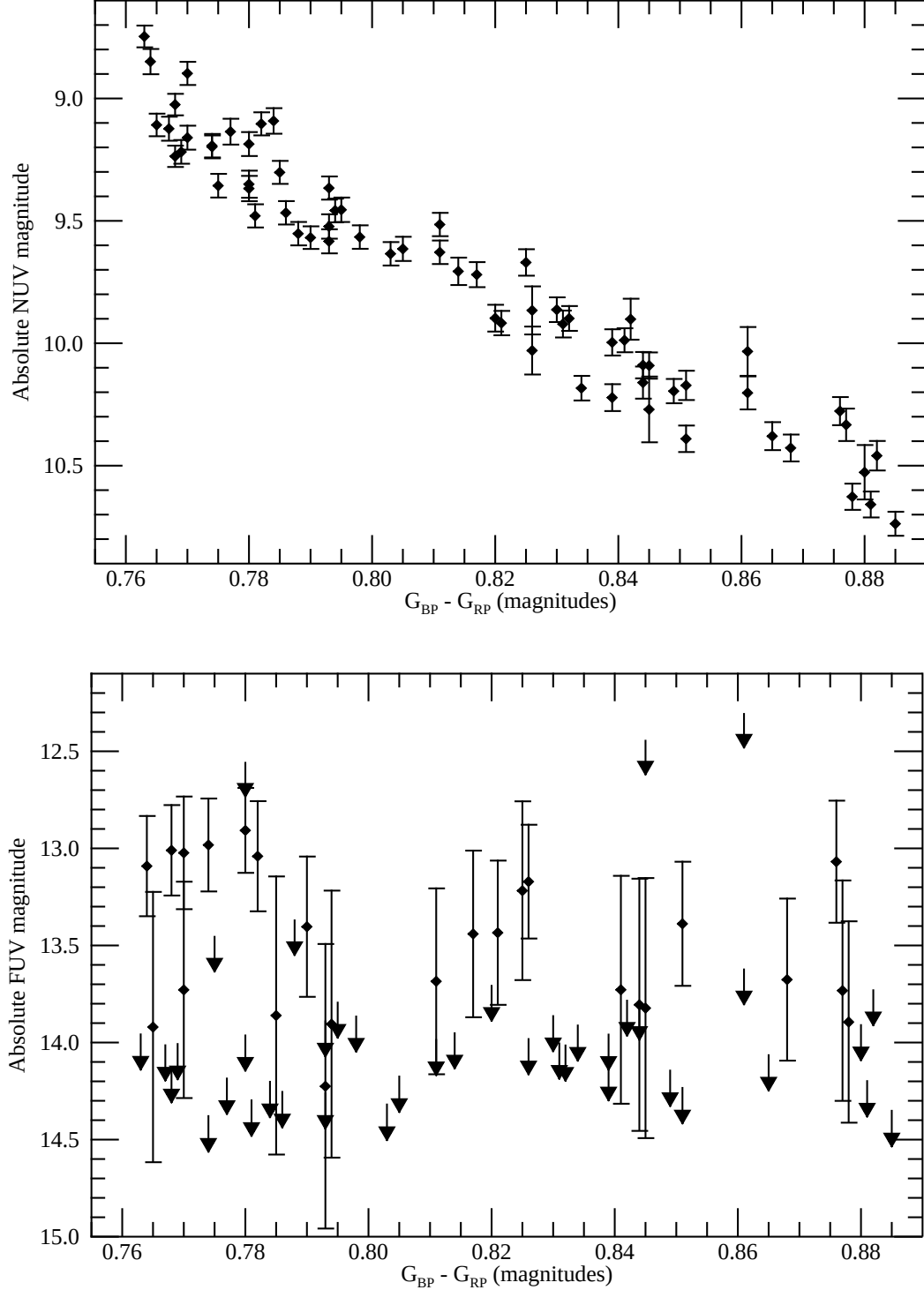
stemming from which epoch is subtracted). The significance of magnitude differences are derived by dividing magnitude differences by the propagated associated uncertainties for both epochs. In this way we produce Figure 3 which plots all valid magnitude differences against their significances.

Figure 3 exhibits a few interesting features. The linear, rising bottom envelope for the data points is set by the significance necessary to detect a magnitude difference given the error distribution in Table 3 (e.g., the smallest  $1\sigma$  is 0.042 magnitudes given the 0.03 magnitude-per-epoch noise floor; see Section 3). Of more interest to the present study is the collection of epoch differences that have significance  $>3\sigma$ . Two stars populate the differences with significance  $>5\sigma$  while 13 stars total (including the two with  $>5\sigma$  differences) contribute to significances  $>3\sigma$ . While the bottom envelope of significances for 3 and  $5\sigma$  are roughly 0.13 and 0.21 magnitudes respectively, some stars appear to have differences up to 0.3 magnitudes.

Appendix A showcases the epochal lightcurves for a sample of stars with significant differences as a sanity check of whether or not their apparent variability is evidence of activity cycles (the most likely variability mechanism to cause changes over the epoch timescales from Table 2). The plots demonstrate that for the two stars with  $>5\sigma$  differences the magnitude changes can be traced back to one discrepant epoch. However, in the lingering  $>3\sigma$  difference sample and evident in the  $2-3\sigma$  population is a set of stars which present tentative (weak) evidence for possible activity cycle variations at the 0.1-0.3 magnitude level.

The weak evidence for variability at an intra-object level makes one wonder if the vertical spread of magnitudes seen in the color-absolute NUV magnitude plot shown in the top panel of Figure 2 could be evidence for variability at an inter-object level since the spread is comparable to the possible cycle variability discussed in the previous paragraph. Curtis (2017) provides evidence for variable interstellar Ca II absorption across the M67 cluster, but it is not clear if ISM structure could





**Figure 2.** *GALEX* and *Gaia* DR3 Hertzsprung-Russell diagrams for Table 1 M67 Solar-type targets. Aperture corrections as listed for each source in Table 3 have been applied. Data points are not corrected for reddening (Taylor 2007 reports an  $E(B-V)$  for M67 of  $41 \pm 4$  mmag; see Curtis 2017 and references therein for a discussion of intervening interstellar medium material on an individual target level). The absolute NUV magnitude is calculated from the weighted mean of all epochs reported in Table 3 for each target and the *Gaia* parallax reported in Table 1. Errors for the absolute NUV magnitude include both the uncertainty on the weighted mean (with a noise floor of 0.03 magnitudes, see Section 3) and the *Gaia* parallax uncertainty; absolute NUV magnitude error bars are typically around 0.05 magnitudes. In general, a spread of roughly 0.3-0.4 magnitudes is seen at each  $G_{BP}-G_{RP}$  color. The absolute FUV magnitude is calculated from the integrated FUV magnitude reported in Table 3 and the *Gaia* parallax; see Section 3 for a description of FUV values and associated uncertainties or limits. Errors on the *Gaia* color are  $<1\%$  and not plotted to maintain clarity.

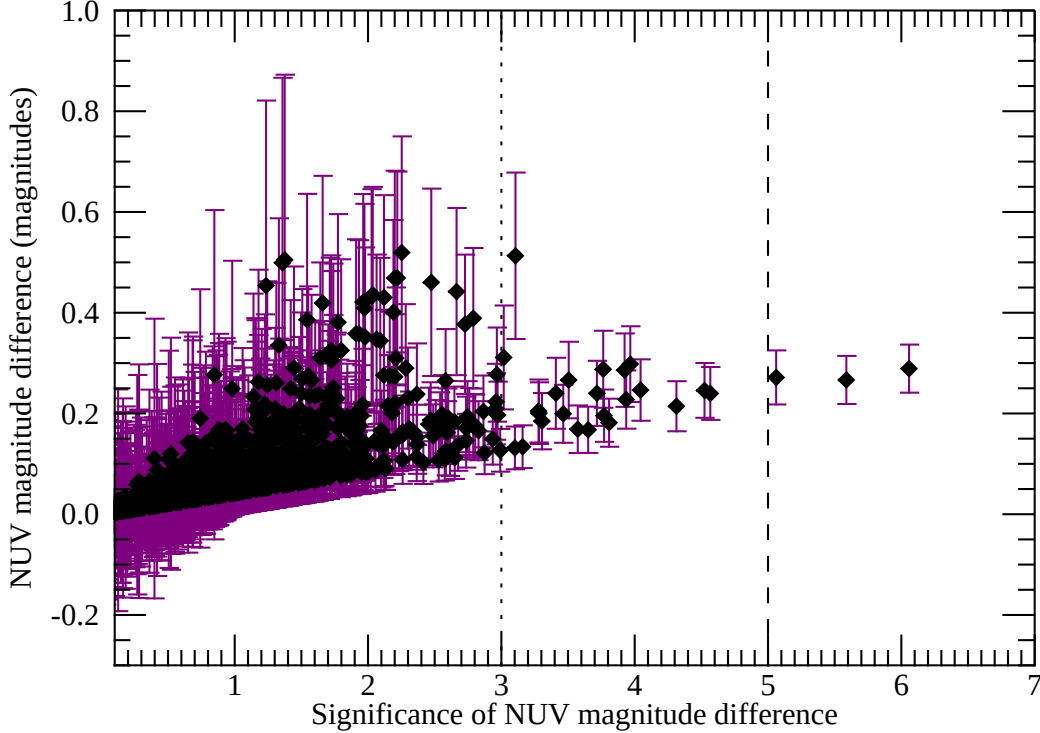


**Figure 3.** NUV magnitude differences between pairs of epochs for a given star plotted as a function of the significance of that magnitude difference (calculated as the magnitude difference value divided by the propagated uncertainty for the two epochs); results for all epoch pairs for all stars in the sample are plotted. Black diamonds are the magnitude difference values while the purple error bars show the propagated uncertainty; dotted and dashed lines guide the eye for assessing  $>3\sigma$  and  $>5\sigma$  significance levels respectively. A collection of epoch pairs appear to show  $>3\sigma$  significance at the 0.1-0.3 magnitude level; see detailed discussion in Section 4.

produce the the 0.3-0.4 magnitude spread in absolute NUV magnitudes seen for each color in Figure 2. Spreads of  $\approx 0.2$  magnitudes are seen in the absolute  $G_{\text{mag}}$  distribution (e.g., Figure 1) which seems to argue against both of ISM and activity as the cause (activity-related variability for the Sun in the visible is  $<1\%$  or  $<0.01$  magnitudes and NUV and visible extinctions should not be of comparable magnitude). The color-absolute FUV magnitude plot shown in the bottom panel of Figure 2 is unable to add much to this discussion given the generally low detection rate and poor signal-to-noise when detections were possibly present. However, one curious feature of the color-absolute FUV diagram is the apparent dichotomy between what appear to be robust detections (sources with absolute FUV magnitudes near 13) and non-detections (sources with limits between 14-14.5 magnitudes) for the bluest Sun-like M67 stars. Taken at face value this could possibly be suggestive of stars with similar physical properties having a spread of greater than a factor of 3 in FUV flux or it could indicate dramatic local reddening variations within the cluster. While tantalizing, the low quality of the FUV detections within the M67 Sun-like star population prevents any conclusive analysis. Thus, while both Figure 2 and epochal lightcurve properties for individual M67 Sun-like stars seem to be suggestive of NUV variability at the  $\sim 0.3$  magnitude level, the available data are unfortunately insufficient to conclusively identify it.

Moving from long-term to short-term variability, we search for evidence of flares in *GALEX* data for our M67 target stars using the 50-second cadence lightcurves. For each object we calculate the median magnitude and median uncertainty from all acceptable lightcurve samples; we exclude

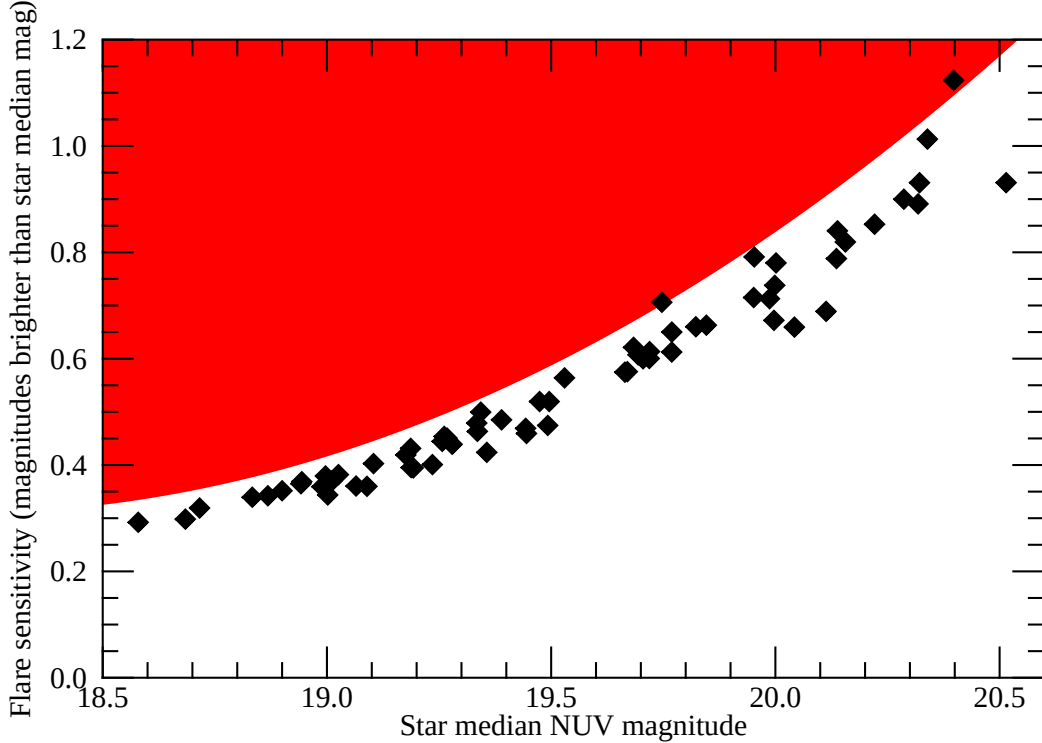


**Figure 4.** NUV flare sensitivity as derived from lightcurve analysis described in Section 4; flare sensitivity is defined to be  $2\times$  the median uncertainty in the lightcurve for each object. The red filled region denotes where our sensitivity allowed us to detect flares but none were seen. Each data point corresponds to a single analyzed star; uncertainties on the median NUV magnitude are omitted for clarity and are generally in the range of 0.03-0.05 magnitudes.

samples which had  $<25$  seconds of integration time and those which featured any data quality flags as output by gPhoton.

We first performed an automated flare search which requires two contiguous data points to be brighter than the median magnitude by  $>2\times$  the median uncertainty for a given star. This returned no positive hits indicating no flares in the dataset as we had defined them. We then performed a visual inspection of all flare lightcurves to ensure this result was robust. The visual inspection returned the same result and demonstrated that all lightcurves generally featured well-behaved magnitude distributions that were consistently contained within the  $\pm 2\times$  median uncertainty bounds (see Appendix A).

Using the  $2\times$  median uncertainty as our detection threshold, we assessed the overall flare sensitivity for each M67 star in our sample. Figure 4 illustrates this sensitivity and in particular how it varies as a function of the target star median NUV magnitude. The range in sensitivities spans from flares that are roughly  $1.3\times$  the stellar NUV flux output on the bright end to flares that are roughly  $3\times$  the stellar NUV flux output on the faint end.

## 5. DISCUSSION AND CONCLUSIONS

We have presented a comprehensive search for ultraviolet variability in the *GALEX* M67 Sun-like star population. Our efforts have failed to identify clear evidence for variability at any observed timescale, but are possibly suggestive of long-term changes likely related to activity cycles if real.

For context we consider the continuum variability of the Sun in the near-ultraviolet. As stated previously, the Sun can experience activity cycle variability on the order of a few percent (roughly 0.03 magnitudes) from 2000-3000 Å and 10-20% (roughly 0.1-0.2 magnitudes) from 1500-2000 Å;

Figure 13(b) of Ayres (2020) illustrates this well. Recall the *GALEX* NUV bandpass spanned 1771-2831 Å, so it would have mostly sampled the 2000-3000 Å region and with our assessed long-term variability sensitivity limit of  $\gtrsim 0.13$  magnitudes (see above) would have been unlikely to detect the roughly few percent Solar-like activity cycle variability amplitudes. If M67 Sun-like stars indeed experience activity cycle variability at the level of 0.3 magnitudes as discussed above, then they would be quite distinct from the Sun in activity properties (roughly ten times the Solar activity cycle variability amplitude in the NUV). The sunspot cycle has a period of  $\approx 11$  years and *GALEX* M67 monitoring epochs feature close to yearly measurements over  $\approx 5$  years. If M67 stars have activity cycle periods similar to the Sun (and have the necessary variability amplitudes much stronger than the Sun so that *GALEX* could detect them), then with a sample of over 60 objects (and assuming random relative phases for their activity cycles across the sample) we would be likely to catch at least some progressing from their activity maximum (or minimum) to their activity minimum (or maximum) over a 5 year time span resulting in the largest possible change in flux. No such changes are conclusively detected and whether this is due to longer activity cycle periods or lower amplitudes (or both) remains unknown (but see more about M67 star activity cycles below).

Few other Sun-like stars have sufficient NUV monitoring data sets available to assess their variability on activity cycle timescales. While Ayres (2021) showcases NUV spectroscopic data for  $\alpha$  Cen A+B and Procyon, he concludes that the continuum measurements are unreliable due to variable narrow-slit throughput and thus does not assess NUV continuum variability. FUV data for  $\alpha$  Cen A reveals 1506 Å continuum variability over one cycle of  $\approx 8\%$  and hence comparable to what is seen for the Sun. Such results seem in tension with the study of Sofia et al. (1989) which found through *International Ultraviolet Explorer (IUE)* 1715-1915 Å spectroscopic monitoring of  $\alpha$  Cen A  $\sim 20\%$  continuum variability over a 3 year timescale (a small fraction of its  $\sim 20$  year activity cycle). The reality of the *IUE* result remains to be verified, a task we leave to a future effort.

Returning our attention to M67, we consider the Ca II activity monitoring program of Giampapa et al. (2006) which for a sample of M67 Sun-like stars similar to that presented herein uncovered interesting variability properties. They observed their targets over 1996-2002, a total duration comparable to the *GALEX* monitoring reported here. They observe variability in nearly all their targets and in some cases see patterns similar to activity cycles with periods  $> 6$  years. M67 Sun-like star Ca II variability consistently has a higher amplitude than that seen for the Sun, a result that would seem supportive of possible 0.3 magnitude NUV variability in the *GALEX* sample as both should be due to magnetic activity processes and if one activity indicator shows enhanced amplitudes relative to the Sun then it might be plausible for other activity indicators to show similar behavior. We reiterate that we consider such a result inconclusive, but certainly worthy of deeper investigation.

Our flare search results can be directly compared to the extensive assessment of NUV flare events in the *Kepler-GALEX* survey conducted by Brasseur et al. (2019) which featured a sample dominated by Sun-like stars. Specifically, Brasseur et al. (2019) provide context around what ultraviolet flares on such stars would look like (their Figures 3-5 provided impetus for our flare search requirements), their distributions of durations and energies (note that we correct all flare energy values shown in the Brasseur et al. 2019 figures to that radiated in the *GALEX* NUV bandpass only, achieved by multiplying by a factor of 0.132 as described in their Section 3.2.3), and the flare incidence rate as a function of flare integrated energy. Our lightcurve sampling with 50 second time-bins and detection requirement of two consecutive flaring data points effectively limits us to detecting flares with duration of  $\gtrsim 100$  seconds (which happens to coincide with the peak in the flare duration distribution shown in Figure 11 of Brasseur et al. 2019). Figure 13 of Brasseur et al. (2019) shows that flares with such durations can have peak flare flux of anywhere from  $\sim 1$ -1000 $\times$  the stellar quiescent NUV flux level. Such flares generally have NUV energies between  $10^{32}$ - $10^{36}$  erg (Figure 16 of Brasseur et al. 2019 after

correction). Figure 14 of Brasseur et al. (2019) show their recovered flare incidence rate as a function of integrated energy.

We seek to assess whether or not the M67 Sun-like star sample features similar flare incidence rates as the *Kepler-GALEX* survey of Brasseur et al. (2019). For any individual M67 star on its own, with a typical total NUV monitoring time of  $\approx 8,000$  seconds, it is not possible to broach the incidence rates for even the weakest flares ( $\sim 10^{32}$  erg) which are around  $10^{-5}$  flares star $^{-1}$  second $^{-1}$  (our flare rate limit in such a case would be  $\lesssim 10^{-4}$  flares star $^{-1}$  second $^{-1}$ ). However, under the assumption that the magnetic properties of all M67 Sun-like stars are on average the same, we can make our assessment based on the aggregate time spent monitoring the cluster's stars. For such an assumption we find that  $4.716 \times 10^5$  seconds of M67 Sun-like star NUV monitoring were obtained by *GALEX* and our effective flare incidence rate limit across NUV energies of  $10^{32}$ - $10^{36}$  erg is  $\lesssim 2.1 \times 10^{-6}$  flares star $^{-1}$  second $^{-1}$  ( $\lesssim 1$  NUV flare star $^{-1}$  week $^{-1}$ ).

Comparing our flare incidence rate limit to Figure 14 of Brasseur et al. (2019) shows agreement for flare NUV energies of  $\gtrsim 10^{33}$  erg. However, for flares with NUV energies between  $10^{32}$ - $10^{33}$  erg our incidence rate limit should have resulted in the detection of a few to several such flares according to the incidence rates of Brasseur et al. (2019) which range between  $2 \times 10^{-6}$  to  $10^{-5}$  flares star $^{-1}$  second $^{-1}$ . We can think of two possible explanations for this tension: 1) our assumption that treats all M67 Sun-like stars in aggregate is unreasonable (the bifurcated FUV magnitude distribution in the bottom panel of Figure 2 could be evidence for this as it may be suggestive of distinct activity properties within the population); 2) M67 stars are generally older than the flaring population displayed in Figure 14 of Brasseur et al. (2019) and flare rates are depressed for older stars. Age information is not presented in Brasseur et al. (2019) and age-adjacent information like rotation periods are only reported for a small fraction of their survey sample, thus we cannot conclusively explore the second explanation although it seems consistent with optical flaring results presented in Davenport et al. (2019).

The flares explored here are vastly more energetic than the typical M-X class flares observed on the Sun (Figure 21 of Brasseur et al. 2019 and references therein). However, based on the work of Tilley et al. (2019) and references therein, the derived flare rate limits suggest conditions that are unlikely to threaten the habitability of any orbiting Earth-like planets, especially if associated energetic particles do not routinely impact the planet (the likelihood of such impacts is much lower for Earth-like planets that have orbital semi-major axes of  $\approx 1$  AU compared to the M-dwarf habitable-zone planets studied by Tilley et al. 2019).

This work has demonstrated that *GALEX* capabilities and monitoring durations for the M67 cluster were just short of addressing the science goals of this investigation. UVEX is the planned successor to *GALEX* and we briefly discuss how it could deliver on assessing cluster ultraviolet variability properties; we rely on parameters described in Kulkarni et al. (2021) and various updates on the UVEX webpage at the time of writing this article. UVEX is planned to have a prime mission lifetime of 2 years and will survey the entire sky in two bandpasses that resemble the *GALEX* NUV and FUV filters. The wide field-of-view ( $3.5^\circ$ ) and finer resolution than *GALEX* ( $\approx 2''$  compared to  $\approx 5''$ ) will make UVEX an efficient cluster surveying machine. While UVEX is supposed to boast 50-100 $\times$  better sensitivity than *GALEX* in a nominal survey field, it is not yet clear what the photometric repeatability will be (recall that *GALEX* was limited to 0.03 magnitudes repeatability in the NUV band). At present, the prime mission sky survey is slated to cover each point on the sky at a minimum of 10 times with cadences ranging from 12 hours to 6 months. UVEX is expected to feature an extended mission after the 2 year prime mission.

To expand upon the research presented herein UVEX must feature the following characteristics. Photometric repeatability between visits at the  $\lesssim 1\%$  level is critical to detecting long-term activity

cycle variability from Sun-like stars. Clusters must be visited at least once per year over a 5-10 year baseline to probe activity cycle durations comparable to the that of the Sun. It is not clear how UVEX will read-out individual exposures or what the minimum sampling time could be; flares would be best explored with sampling times of  $\lesssim 10$  seconds. To explore flare statistics in a conclusive manner it is essential to accrue a substantial amount of total monitoring time for each cluster. Assuming UVEX observes rich clusters featuring  $\sim 50$  stars per FGKM spectral type bin and obtains 7200 seconds of total monitoring every year (e.g., 8 visits of 900 seconds duration each), this would result in an aggregate of 360,000 seconds of monitoring per year per spectral type bin. Maintaining this observing strategy for a 5 year mission duration would allow flare rates in the  $10^{-7}$  flares star $^{-1}$  second $^{-1}$  regime to be explored. Covering clusters with a wide variety of ages would provide the most comprehensive age-ultraviolet flare rate relation ever constructed; more impressive still is that it would be partitioned into spectral type bins, thus opening up potent use cases for understanding planetary atmosphere evolution and stability.

<sup>1</sup> We thank C. Million for help with interpreting *GALEX* time. We appreciate the referee doing a thor-  
<sup>2</sup> ough reading of the paper and providing thoughtful comments that helped improve it. This work has  
<sup>3</sup> been partially supported by HST-AR-17036.001-A and NASA ADAP grant 80NSSC23K0468. This  
<sup>4</sup> research has made use of the Vizier service. This work has made use of data from the European Space  
<sup>5</sup> Agency (ESA) mission *Gaia* (<https://www.cosmos.esa.int/gaia>), processed by the *Gaia* Data Pro-  
<sup>6</sup> cessing and Analysis Consortium (DPAC, <https://www.cosmos.esa.int/web/gaia/dpac/consortium>).  
<sup>7</sup> Funding for the DPAC has been provided by national institutions, in particular the institutions  
<sup>8</sup> participating in the *Gaia* Multilateral Agreement.

*Facilities:* *GALEX*

*Software:* gPhoton (Million et al. 2016)

## REFERENCES

- Abdurro’uf, Accetta, K., Aerts, C., et al. 2022, ApJS, 259, 35, doi: [10.3847/1538-4365/ac4414](https://doi.org/10.3847/1538-4365/ac4414)
- Airapetian, V. S., Barnes, R., Cohen, O., et al. 2020, International Journal of Astrobiology, 19, 136, doi: [10.1017/S1473550419000132](https://doi.org/10.1017/S1473550419000132)
- Ayres, T. R. 2020, ApJS, 250, 16, doi: [10.3847/1538-4365/aba3c6](https://doi.org/10.3847/1538-4365/aba3c6)
- . 2021, ApJ, 923, 192, doi: [10.3847/1538-4357/ac1fec](https://doi.org/10.3847/1538-4357/ac1fec)
- Baliunas, S. L., Donahue, R. A., Soon, W. H., et al. 1995, ApJ, 438, 269, doi: [10.1086/175072](https://doi.org/10.1086/175072)
- Barkaoui, K., Timmermans, M., Soubkiou, A., et al. 2023, A&A, 677, A38, doi: [10.1051/0004-6361/202346838](https://doi.org/10.1051/0004-6361/202346838)
- Barnes, S. A., Weingrill, J., Fritzewski, D., Strassmeier, K. G., & Platais, I. 2016, ApJ, 823, 16, doi: [10.3847/0004-637X/823/1/16](https://doi.org/10.3847/0004-637X/823/1/16)
- Brasseur, C. E., Osten, R. A., & Fleming, S. W. 2019, ApJ, 883, 88, doi: [10.3847/1538-4357/ab3df8](https://doi.org/10.3847/1538-4357/ab3df8)
- Brucalassi, A., Koppenhoefer, J., Saglia, R., et al. 2017, A&A, 603, A85, doi: [10.1051/0004-6361/201527562](https://doi.org/10.1051/0004-6361/201527562)
- Buccino, A. P., & Mauas, P. J. D. 2008, A&A, 483, 903, doi: [10.1051/0004-6361:20078925](https://doi.org/10.1051/0004-6361:20078925)
- Casamiquela, L., Blanco-Cuaresma, S., Carrera, R., et al. 2019, MNRAS, 490, 1821, doi: [10.1093/mnras/stz2595](https://doi.org/10.1093/mnras/stz2595)
- Curtis, J. L. 2017, AJ, 153, 275, doi: [10.3847/1538-3881/aa72e9](https://doi.org/10.3847/1538-3881/aa72e9)
- Davenport, J. R. A., Covey, K. R., Clarke, R. W., et al. 2019, ApJ, 871, 241, doi: [10.3847/1538-4357/aafb76](https://doi.org/10.3847/1538-4357/aafb76)
- Dorren, J. D., & Guinan, E. F. 1994, ApJ, 428, 805, doi: [10.1086/174289](https://doi.org/10.1086/174289)
- Dravins, D., Linde, P., Ayres, T. R., et al. 1993a, ApJ, 403, 412, doi: [10.1086/172212](https://doi.org/10.1086/172212)
- Dravins, D., Linde, P., Fredga, K., & Gahm, G. F. 1993b, ApJ, 403, 396, doi: [10.1086/172211](https://doi.org/10.1086/172211)
- Floyd, L. E., Cook, J. W., Herring, L. C., & Crane, P. C. 2003, Advances in Space Research, 31, 2111, doi: [10.1016/S0273-1177\(03\)00148-0](https://doi.org/10.1016/S0273-1177(03)00148-0)
- France, K., Loyd, R. O. P., Youngblood, A., et al. 2016, ApJ, 820, 89, doi: [10.3847/0004-637X/820/2/89](https://doi.org/10.3847/0004-637X/820/2/89)



- Gaia Collaboration, Vallenari, A., Brown, A. G. A., et al. 2023, *A&A*, 674, A1, doi: [10.1051/0004-6361/202243940](https://doi.org/10.1051/0004-6361/202243940)
- Geller, A. M., Latham, D. W., & Mathieu, R. D. 2015, *AJ*, 150, 97, doi: [10.1088/0004-6256/150/3/97](https://doi.org/10.1088/0004-6256/150/3/97)
- Geller, A. M., Mathieu, R. D., Latham, D. W., et al. 2021, *AJ*, 161, 190, doi: [10.3847/1538-3881/abdd23](https://doi.org/10.3847/1538-3881/abdd23)
- Giampapa, M. S., Hall, J. C., Radick, R. R., & Baliunas, S. L. 2006, *ApJ*, 651, 444, doi: [10.1086/507624](https://doi.org/10.1086/507624)
- Godolt, M., Grenfell, J. L., Hamann-Reinus, A., et al. 2015, *Planet. Space Sci.*, 111, 62, doi: [10.1016/j.pss.2015.03.010](https://doi.org/10.1016/j.pss.2015.03.010)
- Hourihane, A., François, P., Worley, C. C., et al. 2023, *A&A*, 676, A129, doi: [10.1051/0004-6361/202345910](https://doi.org/10.1051/0004-6361/202345910)
- Ilin, E., Schmidt, S. J., Poppenhäger, K., et al. 2021, *A&A*, 645, A42, doi: [10.1051/0004-6361/202039198](https://doi.org/10.1051/0004-6361/202039198)
- Jönsson, H., Holtzman, J. A., Allende Prieto, C., et al. 2020, *AJ*, 160, 120, doi: [10.3847/1538-3881/aba592](https://doi.org/10.3847/1538-3881/aba592)
- Kamgar, L., France, K., & Youngblood, A. 2024, *PASP*, 136, 024202, doi: [10.1088/1538-3873/ad119f](https://doi.org/10.1088/1538-3873/ad119f)
- Kim, D., Choi, H., & Yi, Y. 2022, *Journal of Korean Astronomical Society*, 55, 59, doi: [10.5303/JKAS.2022.55.2.59](https://doi.org/10.5303/JKAS.2022.55.2.59)
- Kowalski, A. F. 2024, *Living Reviews in Solar Physics*, 21, 1, doi: [10.1007/s41116-024-00039-4](https://doi.org/10.1007/s41116-024-00039-4)
- Krivova, N. A., Solanki, S. K., & Floyd, L. 2006, *A&A*, 452, 631, doi: [10.1051/0004-6361:20064809](https://doi.org/10.1051/0004-6361:20064809)
- Krivova, N. A., Solanki, S. K., Wenzler, T., & Podlipnik, B. 2009, *Journal of Geophysical Research (Atmospheres)*, 114, D00I04, doi: [10.1029/2009JD012375](https://doi.org/10.1029/2009JD012375)
- Kulkarni, S. R., Harrison, F. A., Grefenstette, B. W., et al. 2021, arXiv e-prints, arXiv:2111.15608, doi: [10.48550/arXiv.2111.15608](https://doi.org/10.48550/arXiv.2111.15608)
- Lee, Y. S., Beers, T. C., Sivarani, T., et al. 2008, *AJ*, 136, 2050, doi: [10.1088/0004-6256/136/5/2050](https://doi.org/10.1088/0004-6256/136/5/2050)
- Luo, A. L., Zhao, Y. H., Zhao, G., & et al. 2019, *VizieR Online Data Catalog: LAMOST DR5 catalogs (Luo+, 2019)*, *VizieR On-line Data Catalog: V/164*. Originally published in: 2019RAA..in.prep..L
- Madhusudhan, N., Constantinou, S., Holmberg, M., et al. 2025, *ApJL*, 983, L40, doi: [10.3847/2041-8213/adc1c8](https://doi.org/10.3847/2041-8213/adc1c8)
- Mamajek, E., & Stapelfeldt, K. 2024, arXiv e-prints, arXiv:2402.12414, doi: [10.48550/arXiv.2402.12414](https://doi.org/10.48550/arXiv.2402.12414)
- Metcalfe, T. S., Dziembowski, W. A., Judge, P. G., & Snow, M. 2007, *MNRAS*, 379, L16, doi: [10.1111/j.1745-3933.2007.00325.x](https://doi.org/10.1111/j.1745-3933.2007.00325.x)
- Million, C., Fleming, S. W., Shiao, B., et al. 2016, *ApJ*, 833, 292, doi: [10.3847/1538-4357/833/2/292](https://doi.org/10.3847/1538-4357/833/2/292)
- Million, C. C., Clair, M. S., Fleming, S. W., Bianchi, L., & Osten, R. 2023, *ApJS*, 268, 41, doi: [10.3847/1538-4365/ace717](https://doi.org/10.3847/1538-4365/ace717)
- Morrissey, P., Conrow, T., Barlow, T. A., et al. 2007, *ApJS*, 173, 682, doi: [10.1086/520512](https://doi.org/10.1086/520512)
- Noormohammadi, M., Khakian Ghomi, M., & Haghi, H. 2023, *MNRAS*, 523, 3538, doi: [10.1093/mnras/stad1589](https://doi.org/10.1093/mnras/stad1589)
- Pasquini, L., Brucalassi, A., Ruiz, M. T., et al. 2012, *A&A*, 545, A139, doi: [10.1051/0004-6361/201219169](https://doi.org/10.1051/0004-6361/201219169)
- Randich, S., Gilmore, G., Magrini, L., et al. 2022, *A&A*, 666, A121, doi: [10.1051/0004-6361/202243141](https://doi.org/10.1051/0004-6361/202243141)
- Reyes, C., Stello, D., Hon, M., et al. 2024, *MNRAS*, 532, 2860, doi: [10.1093/mnras/stae1650](https://doi.org/10.1093/mnras/stae1650)
- Rockosi, C. M., Lee, Y. S., Morrison, H. L., et al. 2022, *ApJS*, 259, 60, doi: [10.3847/1538-4365/ac5323](https://doi.org/10.3847/1538-4365/ac5323)
- Smolinski, J. P., Lee, Y. S., Beers, T. C., et al. 2011, *AJ*, 141, 89, doi: [10.1088/0004-6256/141/3/89](https://doi.org/10.1088/0004-6256/141/3/89)
- Sofia, U. J., Bruhweiler, F. C., & Sofia, S. 1989, *J. Geophys. Res.*, 94, 9117, doi: [10.1029/JA094iA07p09117](https://doi.org/10.1029/JA094iA07p09117)
- Soubiran, C., Jasiewicz, G., Chemin, L., et al. 2018, *A&A*, 616, A7, doi: [10.1051/0004-6361/201832795](https://doi.org/10.1051/0004-6361/201832795)
- Spina, L., Ting, Y. S., De Silva, G. M., et al. 2021, *MNRAS*, 503, 3279, doi: [10.1093/mnras/stab471](https://doi.org/10.1093/mnras/stab471)
- Taylor, B. J. 2007, *AJ*, 133, 370, doi: [10.1086/509781](https://doi.org/10.1086/509781)
- Tilley, M. A., Segura, A., Meadows, V., Hawley, S., & Davenport, J. 2019, *Astrobiology*, 19, 64, doi: [10.1089/ast.2017.1794](https://doi.org/10.1089/ast.2017.1794)
- Wilson, D. J., Froning, C. S., Duvvuri, G. M., et al. 2025, *ApJ*, 978, 85, doi: [10.3847/1538-4357/ad9251](https://doi.org/10.3847/1538-4357/ad9251)

## APPENDIX

## A. EPOCHAL AND FLARE LIGHTCURVE EXAMPLES

In this Appendix we show example figures of stars whose epochal lightcurves either appear to show variability or had  $>3\sigma$  magnitude differences between epochs (Figure 5). Two example flare lightcurve segments are also shown (Figure 6).

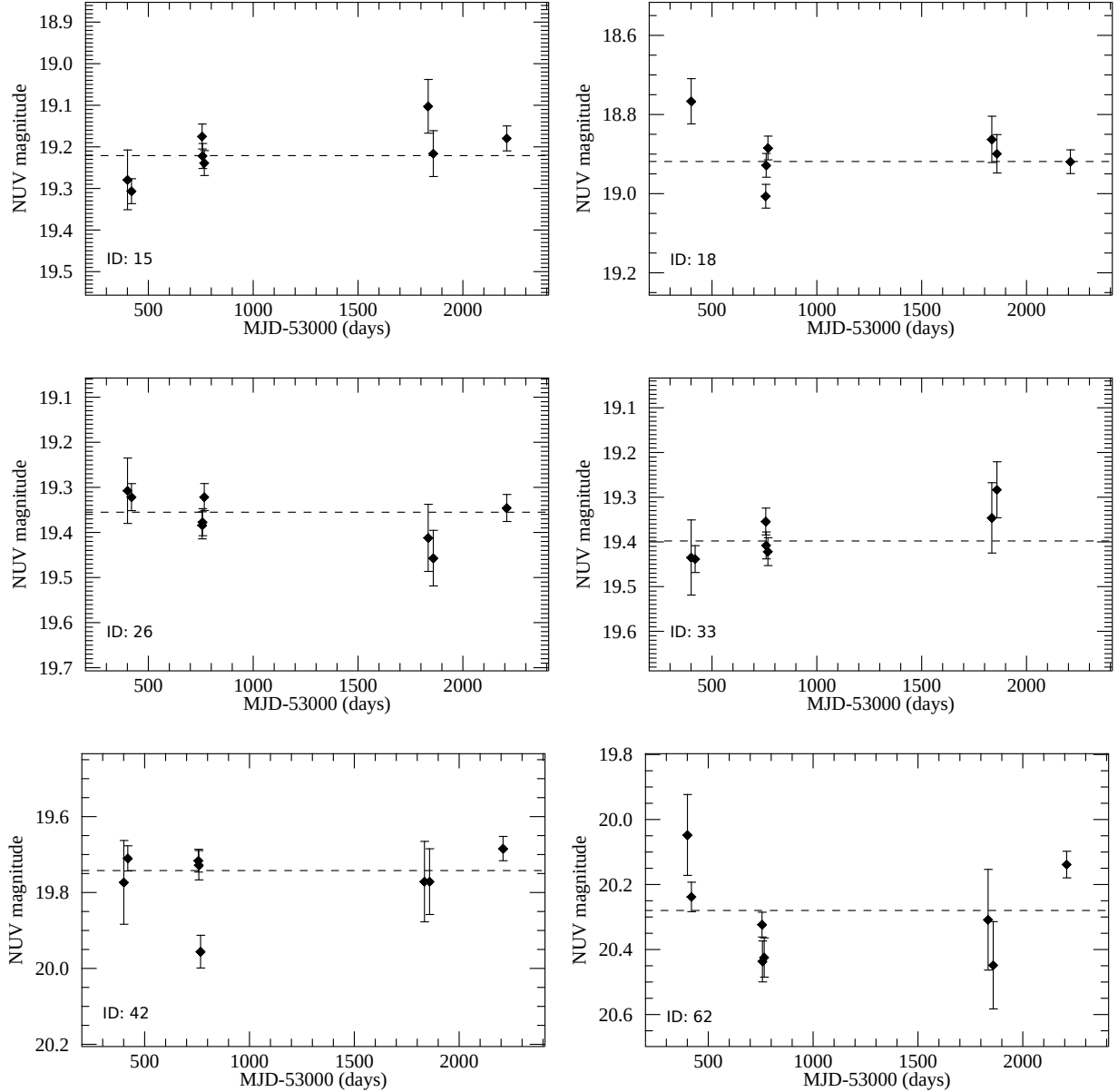


**Figure 5.** Example epochal lightcurves; NUV magnitudes do not have aperture corrections applied. The dashed line in each figure panel shows the weighted mean NUV magnitude calculated from all epochs. Star 42 is an example of a star with  $>5\sigma$  difference between two epochs, in this case caused by one data point. One other star shares such characteristics. Stars 15, 18, and 62 have  $3\text{--}5\sigma$  differences between two epochs and also appear to have weak evidence for long-term variability like what one would expect for an activity cycle with period  $\gtrsim 5$  years. Stars 26 and 33 have  $2\text{--}3\sigma$  evidence for long-term variability from what could be an activity cycle.

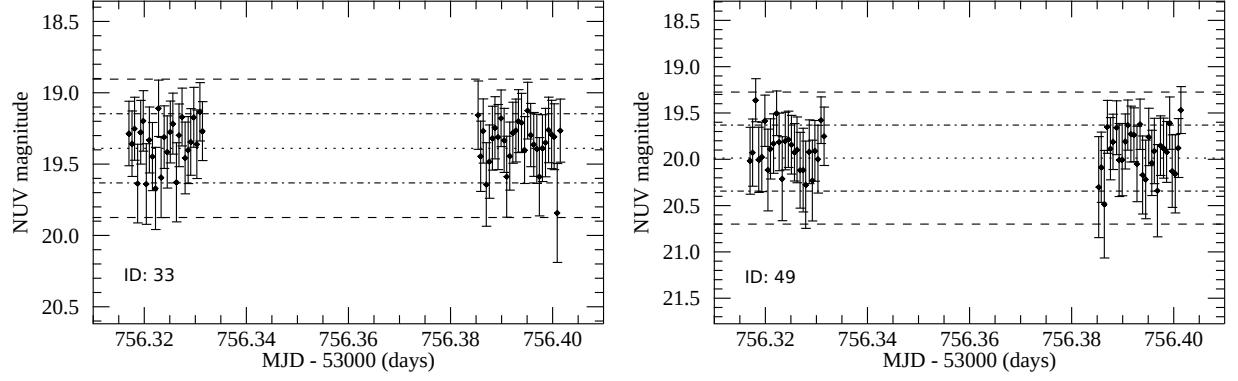


**Figure 6.** Example flare lightcurves zoomed in on Epoch 3 time regions (see Table 2); NUV magnitudes do not have aperture corrections applied. The dotted line in each figure panel shows the median NUV magnitude calculated from all flare lightcurve samples. The dash-dotted curves show the median magnitude value  $\pm 1 \times$  the median uncertainty value from all samples and the dashed curve  $\pm 2 \times$  this value.

**Table 3.** *GALEX* Photometry

ID	Ap. Rad. (")	Annulus Rad. (")	NUV Ap. Corr. (mag)	FUV Ap. Corr. (mag)	NUV Epoch (MJD)	NUV Mag.	NUV Mag. Error	FUV Epoch (MJD)	FUV Mag.	FUV Mag. Error
1	12.8	16.0,22.0	0.090	0.090	53400.5808	18.674	0.054	53724.6400	23.792	—
					53419.5908	18.588	0.030			
					53756.3515	18.571	0.030			
					53758.3800	18.570	0.030			
					53766.7386	18.576	0.030			
					54834.4817	18.559	0.049			
					54858.8591	18.606	0.040			
2	12.8	16.0,22.0	0.090	0.090	55209.2056	18.576	0.030	54066.7562	22.898	0.254
					53400.5815	18.685	0.051			
					53756.3531	18.635	0.030			
					53758.3799	18.648	0.030			
					53766.7386	18.682	0.030			
3	12.8	16.0,22.0	0.090	0.090	54526.6951	18.651	0.030	53672.1145	23.772	0.695
					53419.5907	18.955	0.030			
					53756.3527	18.936	0.030			
					53758.3800	18.952	0.030			
					53766.7385	18.973	0.030			
4	12.8	16.0,22.0	0.090	0.090	53781.7254	19.034	0.085	53746.8819	23.749	—
					54493.4772	19.054	0.081			
					53400.5823	18.790	0.057			
					53419.5908	18.882	0.030			
					53756.3513	18.886	0.030			
					53758.3799	18.861	0.030			
					53766.7386	18.855	0.030			
5	12.8	16.0,22.0	0.090	0.090	54834.4817	18.832	0.057	53907.8103	22.796	0.230
					54858.8590	18.873	0.047			
					55209.2056	18.844	0.030			
					53400.5761	18.883	0.061			
6	12.8	16.0,22.0	0.090	0.090	54834.4817	18.790	0.054	53683.3491	23.872	—
					54858.8590	18.766	0.045			
					55209.2056	18.820	0.030			
					53419.5908	19.020	0.030			
	12.8	16.0,22.0	0.090	0.090	53756.3526	18.991	0.030	53683.3491	23.872	—
					53758.3799	18.979	0.030			
					53766.7386	18.950	0.030			

**Table 3** *continued on next page*

**Table 3** (*continued*)

ID	Ap. Rad. (")	Annulus Rad. (")	NUV Ap. Corr. (mag)	FUV Ap. Corr. (mag)	NUV Epoch (MJD)	NUV Mag.	NUV Mag. Error	FUV Epoch (MJD)	FUV Mag.	FUV Mag. Error
7	12.8	16.0,22.0	0.090	0.090	53419.5906	18.979	0.030	53726.8109	23.801	—
					53756.3498	18.999	0.030			
					53758.3800	19.043	0.030			
					53766.7387	19.034	0.030			
8	12.8	16.0,22.0	0.090	0.090	53419.5907	18.753	0.030	53725.2104	22.849	0.287
					53756.3526	18.722	0.030			
					53758.3800	18.697	0.030			
					53766.7386	18.723	0.030			
9	12.8	16.0,22.0	0.090	0.090	53400.5804	18.936	0.063	53739.6427	23.463	0.555
					53419.5908	18.953	0.030			
					53756.3505	18.910	0.030			
					53758.3800	18.863	0.030			
					53766.7384	18.894	0.030			
					54834.4817	18.927	0.061			
					54858.8591	18.846	0.047			
10	9.0	12.8,18.8	0.130	0.100	55209.2057	18.851	0.030	53744.8282	24.154	—
					53400.5787	19.057	0.062			
					53419.5908	18.997	0.030			
					53756.3518	19.006	0.030			
					53758.3801	18.979	0.030			
					53766.7386	18.997	0.030			
					54834.4817	19.089	0.061			
11	12.8	16.0,22.0	0.090	0.090	54858.8590	18.998	0.047	53822.1235	22.767	0.236
					55209.2056	18.999	0.030			
					53400.5871	18.971	0.055			
					53419.5908	18.994	0.030			
					54834.4793	18.938	0.046			
12	12.8	16.0,22.0	0.090	0.090	54858.8558	18.990	0.036	53537.8577	23.249	—
					55208.2469	18.985	0.030			
					55209.2054	18.982	0.030			
					53419.5908	19.162	0.030			
					53781.7255	19.048	0.083			
					54493.4773	19.155	0.089			

**Table 3** *continued on next page*

**Table 3** (*continued*)

ID	Ap. Rad. (")	Annulus Rad. (")	NUV Ap. Corr. (mag)	FUV Ap. Corr. (mag)	NUV Epoch (MJD)	NUV Mag.	NUV Mag. Error	FUV Epoch (MJD)	FUV Mag.	FUV Mag. Error
13	9.0	12.8,18.8	0.130	0.100	53400.5805	19.000	0.061	53745.3082	24.075	—
					53419.5906	19.043	0.030			
					53756.3528	19.067	0.030			
					53758.3801	19.055	0.030			
					53766.7387	19.095	0.030			
					54834.4817	19.168	0.066			
					54858.8591	19.039	0.049			
14	12.8	16.0,22.0	0.090	0.090	55209.2056	19.030	0.030	53993.6717	22.741	0.215
					53400.5803	19.046	0.047			
					53756.3532	19.020	0.030			
					53758.3801	18.951	0.030			
					53766.7387	19.019	0.030			
					54526.6951	19.010	0.030			
					54834.4817	18.983	0.063			
15	9.0	12.8,18.8	0.130	0.100	54858.8591	19.148	0.059	53749.7145	23.784	—
					55209.2056	19.064	0.030			
					53400.5809	19.279	0.071			
					53419.5910	19.306	0.030			
					53756.3528	19.175	0.030			
					53758.3801	19.221	0.030			
					53766.7386	19.238	0.030			
16	12.8	16.0,22.0	0.090	0.090	54834.4817	19.102	0.064	54639.3843	22.407	—
					54858.8590	19.216	0.055			
					55209.2058	19.179	0.030			
					53400.5843	19.164	0.067			
17	9.0	12.8,18.8	0.130	0.100	54834.4771	19.249	0.078	53723.9953	24.023	—
					54858.8523	19.281	0.061			
					55208.2470	19.171	0.030			
					53400.5657	19.381	0.110			
					53419.5908	19.235	0.030			
					53756.3503	19.225	0.030			
					53758.3801	19.272	0.030			
					53766.7386	19.242	0.030			
					54834.4817	19.368	0.073			
					54858.8590	19.192	0.053			
					55209.2058	19.201	0.030			

**Table 3** *continued on next page*



**Table 3** (*continued*)

ID	Ap. Rad. (")	Annulus Rad. (")	NUV Ap. Corr. (mag)	FUV Ap. Corr. (mag)	NUV Epoch (MJD)	NUV Mag.	NUV Mag. Error	FUV Epoch (MJD)	FUV Mag.	FUV Mag. Error
18	12.8	16.0,22.0	0.090	0.090	53400.5812	18.766	0.057	53764.9489	22.855	0.281
					53756.3529	19.006	0.030			
					53758.3800	18.928	0.030			
					53766.7385	18.884	0.030			
					54834.4817	18.862	0.058			
					54858.8590	18.899	0.048			
					55209.2057	18.919	0.030			
19	9.0	12.8,18.8	0.130	0.100	53400.5830	19.107	0.063	53756.5656	24.155	—
					53419.5907	19.065	0.030			
					53756.3533	19.133	0.030			
					53758.3801	19.070	0.030			
					53766.7387	19.081	0.030			
					54834.4817	19.019	0.057			
					54858.8590	19.075	0.049			
20	12.8	16.0,22.0	0.090	0.090	55209.2055	19.054	0.030	53733.2116	23.662	0.715
					53419.5906	19.154	0.030			
					53756.3516	19.071	0.030			
					53758.3801	19.093	0.030			
21	9.0	12.8,18.8	0.130	0.100	53766.7387	19.095	0.030	53727.0087	24.015	—
					53419.5907	19.257	0.030			
					53756.3504	19.264	0.030			
					53758.3800	19.265	0.030			
22	12.8	16.0,22.0	0.090	0.090	53766.7387	19.258	0.030	53438.2583	23.128	—
					53419.5908	19.324	0.030			
					53781.7255	19.164	0.093			
23	12.8	16.0,22.0	0.090	0.090	54493.4772	19.301	0.097	53694.4316	23.141	0.359
					53419.5907	19.320	0.030			
					53756.3553	19.326	0.030			
					53758.3870	18.821	0.366			
24	12.8	16.0,22.0	0.090	0.090	53766.7384	19.275	0.030	53684.4023	23.717	—
					53419.5907	19.150	0.030			
					53756.3500	19.200	0.030			
					53758.3800	19.210	0.030			
25	9.0	12.8,18.8	0.130	0.100	53766.7386	19.215	0.030	53690.9847	24.090	0.731
					53419.5909	19.495	0.030			
					53781.7255	19.441	0.098			
					54493.4772	19.364	0.089			

**Table 3** *continued on next page*

**Table 3** (*continued*)

ID	Ap. Rad. (")	Annulus Rad. (")	NUV Ap. Corr. (mag)	FUV Ap. Corr. (mag)	NUV Epoch (MJD)	NUV Mag.	NUV Mag. Error	FUV Epoch (MJD)	FUV Mag.	FUV Mag. Error
26	9.0	12.8,18.8	0.130	0.090	53400.5811	19.307	0.072	53755.9153	24.049	—
					53419.5910	19.321	0.030			
					53756.3538	19.384	0.030			
					53758.3799	19.377	0.030			
					53766.7386	19.321	0.030			
					54834.4816	19.412	0.074			
					54858.8590	19.457	0.061			
27	12.8	16.0,22.0	0.090	0.090	55209.2057	19.345	0.030	53677.5910	23.708	0.686
					53419.5909	19.336	0.030			
					53756.3542	19.227	0.030			
					53758.3800	19.202	0.030			
					53766.7386	19.278	0.030			
					53781.7255	19.281	0.098			
28	12.8	16.0,22.0	0.090	0.090	54493.4772	19.244	0.093	53732.3388	23.592	—
					53400.5797	19.261	0.079			
					53419.5909	19.261	0.030			
					53756.3522	19.265	0.030			
					53758.3800	19.246	0.030			
					53766.7386	19.295	0.030			
					54834.4816	19.244	0.077			
29	12.8	16.0,22.0	0.090	0.090	54858.8591	19.090	0.054	53710.7620	23.628	—
					55209.2054	19.252	0.030			
					53400.5788	19.282	0.080			
					53419.5909	19.355	0.030			
					53756.3512	19.302	0.030			
					53758.3801	19.371	0.031			
					53766.7386	19.364	0.031			
30	9.0	12.8,18.8	0.130	0.100	54834.4817	19.437	0.091	53704.9255	24.081	—
					54858.8590	19.220	0.063			
					55209.2056	19.283	0.030			
					53419.5908	19.423	0.030			
					53756.3501	19.401	0.030			
					53758.3800	19.445	0.030			
					53766.7387	19.453	0.030			

**Table 3** *continued on next page*

**Table 3** (*continued*)

ID	Ap. Rad. (")	Annulus Rad. (")	NUV Ap. Corr. (mag)	FUV Ap. Corr. (mag)	NUV Epoch (MJD)	NUV Mag.	NUV Mag. Error	FUV Epoch (MJD)	FUV Mag.	FUV Mag. Error
31	9.0	12.8,18.8	0.130	0.100	53400.5800	19.619	0.095	53715.9788	23.945	—
					53419.5908	19.439	0.030			
					53756.3520	19.398	0.030			
					53758.3800	19.388	0.030			
					53766.7387	19.423	0.030			
					54834.4817	19.547	0.090			
					54858.8590	19.435	0.064			
32	12.8	16.0,22.0	0.090	0.090	55209.2056	19.403	0.030	53671.4059	23.725	—
					53419.5908	19.255	0.030			
					53756.3509	19.244	0.030			
					53758.3800	19.237	0.030			
33	12.8	16.0,22.0	0.090	0.090	53766.7385	19.289	0.030	53734.4397	23.454	0.477
					53400.5821	19.434	0.084			
					53419.5907	19.438	0.030			
					53756.3537	19.354	0.030			
					53758.3800	19.407	0.030			
					53766.7386	19.421	0.031			
34	12.8	16.0,22.0	0.090	0.090	54834.4816	19.346	0.078	53739.6362	23.740	—
					54858.8590	19.283	0.062			
					53400.5781	19.472	0.088			
					53419.5909	19.520	0.030			
					53756.3534	19.516	0.030			
					53758.3800	19.529	0.032			
					53766.7386	19.470	0.030			
35	12.8	16.0,22.0	0.090	0.090	54834.4817	19.454	0.084	53742.1204	23.223	0.427
					54858.8591	19.336	0.062			
					55209.2056	19.493	0.030			
					53400.5801	19.620	0.100			
					53419.5909	19.420	0.030			
					53756.3507	19.528	0.030			
					53758.3800	19.495	0.033			
					53766.7385	19.709	0.037			
					54834.4817	19.432	0.085			
					54858.8590	19.421	0.066			
					55209.2057	19.443	0.030			

**Table 3** *continued on next page*

**Table 3** (*continued*)

ID	Ap. Rad. (")	Annulus Rad. (")	NUV Ap. Corr. (mag)	FUV Ap. Corr. (mag)	NUV Epoch (MJD)	NUV Mag.	NUV Mag. Error	FUV Epoch (MJD)	FUV Mag.	FUV Mag. Error
36	12.8	16.0,22.0	0.090	0.090	53400.5820	19.878	0.125	53758.8910	23.514	—
					53419.5908	19.651	0.030			
					53756.3488	19.698	0.030			
					53758.3798	19.743	0.038			
					53766.7387	19.722	0.037			
					54834.4816	19.803	0.111			
					54858.8591	19.698	0.078			
37	12.8	16.0,22.0	0.090	0.090	55209.2054	19.711	0.031	53671.1922	23.224	0.369
					53419.5907	19.712	0.032			
					53756.3508	19.656	0.030			
					53758.3797	19.794	0.041			
38	12.8	16.0,22.0	0.090	0.090	53766.7385	19.712	0.037	53738.1815	23.077	0.458
					53400.5808	19.679	0.115			
					53419.5906	19.513	0.030			
					53756.3516	19.534	0.030			
					53758.3799	19.608	0.037			
					53766.7386	19.513	0.034			
					54834.4817	19.562	0.101			
39	12.8	16.0,22.0	0.090	0.090	54858.8590	19.485	0.075	53660.6867	22.957	0.289
					55209.2056	19.495	0.030			
40	12.8	16.0,22.0	0.090	0.090	53781.7254	19.655	0.128	53669.7811	23.783	—
					54493.4772	19.649	0.120			
					53419.5909	19.831	0.034			
					53756.3518	19.803	0.030			
41	12.8	16.0,22.0	0.090	0.090	53758.3799	19.899	0.043	53674.6626	23.698	—
					53766.7386	19.832	0.040			
					53419.5908	19.780	0.034			
					53756.3521	19.613	0.030			
42	12.8	16.0,22.0	0.090	0.090	53758.3800	19.715	0.038	53724.5434	23.823	—
					53766.7388	19.721	0.037			
					53400.5822	19.773	0.110			
					53419.5908	19.710	0.033			
					53756.3510	19.716	0.030			
					53758.3800	19.728	0.038			
					53766.7392	19.955	0.043			
					54834.4816	19.771	0.105			
					54858.8589	19.771	0.086			
					55209.2056	19.684	0.031			

**Table 3** *continued on next page*

**Table 3** (*continued*)

ID	Ap. Rad. (")	Annulus Rad. (")	NUV Ap. Corr. (mag)	FUV Ap. Corr. (mag)	NUV Epoch (MJD)	NUV Mag.	NUV Mag. Error	FUV Epoch (MJD)	FUV Mag.	FUV Mag. Error
43	12.8	16.0,22.0	0.090	0.090	53400.5810	19.736	0.108	53737.7852	23.763	—
					53419.5909	19.652	0.031			
					53756.3529	19.640	0.030			
					53758.3802	19.684	0.036			
					53766.7387	19.728	0.037			
					54834.4817	19.734	0.104			
					54858.8590	19.461	0.066			
44	12.8	16.0,22.0	0.090	0.090	55209.2057	19.602	0.031	53686.9041	23.731	—
					53419.5908	20.069	0.044			
					53756.3541	19.986	0.031			
					53758.3800	19.957	0.044			
					53766.7385	20.052	0.049			
					53781.7255	19.818	0.137			
					54493.4772	19.962	0.157			
45	12.8	16.0,22.0	0.090	0.090	53400.5798	19.852	0.113	53759.9105	23.696	—
					53419.5905	19.778	0.034			
					53756.3519	19.712	0.030			
					53758.3800	19.735	0.038			
					53766.7385	19.689	0.036			
					54834.4817	19.897	0.116			
					54858.8591	19.660	0.075			
46	12.8	16.0,21.0	0.090	0.090	55209.2056	19.756	0.032	53721.1998	23.839	—
					53400.5808	20.395	0.208			
					53419.5908	19.963	0.042			
					53756.3527	19.926	0.031			
					53758.3799	19.973	0.048			
					53766.7386	19.959	0.046			
					54834.4817	20.284	0.182			
47	12.8	16.0,22.0	0.090	0.090	54858.8590	19.875	0.097	53707.7909	23.466	0.585
					55209.2053	19.926	0.041			
					53419.5908	19.723	0.033			
					53756.3508	19.686	0.030			
					53758.3799	19.767	0.038			
					53766.7385	19.749	0.037			

**Table 3** *continued on next page*

**Table 3** (*continued*)

ID	Ap. Rad. (")	Annulus Rad. (")	NUV Ap. Corr. (mag)	FUV Ap. Corr. (mag)	NUV Epoch (MJD)	NUV Mag.	NUV Mag. Error	FUV Epoch (MJD)	FUV Mag.	FUV Mag. Error
48	12.8	16.0,22.0	0.090	0.090	53400.5789	19.677	0.107	53740.6074	23.535	—
					53419.5907	19.653	0.032			
					53756.3527	19.671	0.030			
					53758.3800	19.686	0.039			
					53766.7385	19.684	0.038			
					54834.4817	19.870	0.123			
					54858.8591	19.670	0.084			
49	12.8	16.0,22.0	0.090	0.090	55209.2055	19.580	0.030	53722.1705	23.653	0.647
					53419.5911	19.888	0.036			
					53756.3515	19.889	0.030			
					53758.3798	19.993	0.046			
50	12.8	16.0,22.0	0.090	0.090	53766.7386	20.089	0.049	53746.8675	23.583	—
					53400.5772	19.780	0.108			
					53419.5908	19.932	0.037			
					53756.3509	19.943	0.030			
					53758.3797	19.986	0.046			
					53766.7386	19.974	0.044			
					54834.4817	20.132	0.141			
51	12.8	16.0,22.0	0.090	0.090	54858.8590	19.931	0.089	53705.0204	23.566	0.668
					55209.2055	19.894	0.036			
					53400.5814	19.788	0.111			
					53419.5909	19.791	0.034			
					53756.3511	19.863	0.030			
					53758.3801	19.902	0.043			
					53766.7386	19.844	0.041			
52	12.8	16.0,22.0	0.090	0.090	54834.4817	19.936	0.126	53781.7255	22.320	—
					54858.8589	19.701	0.080			
53	12.8	16.0,22.0	0.090	0.090	55209.2058	19.812	0.034	54443.5320	23.443	—
					53781.7255	20.253	0.198			
					54493.4773	20.063	0.162			
					53400.5820	20.145	0.130			
					54526.6953	20.012	0.039			

**Table 3** *continued on next page*



**Table 3** (*continued*)

ID	Ap. Rad. (")	Annulus Rad. (")	NUV Ap. Corr. (mag)	FUV Ap. Corr. (mag)	NUV Epoch (MJD)	NUV Mag.	NUV Mag. Error	FUV Epoch (MJD)	FUV Mag.	FUV Mag. Error
54	12.8	16.0,22.0	0.090	0.090	53400.5752	19.941	0.123	53796.9392	23.922	—
					53419.5907	19.929	0.038			
					53756.3494	20.027	0.031			
					53758.3798	20.024	0.047			
					53766.7386	20.105	0.050			
					54834.4817	20.371	0.161			
					54858.8590	19.911	0.092			
55	9.0	12.8,18.8	0.130	0.100	55209.2056	19.858	0.034	53724.5505	23.217	0.315
					53400.5816	19.817	0.096			
					53419.5908	20.128	0.037			
					53756.3544	20.055	0.030			
					53758.3800	19.933	0.036			
					53766.7388	19.982	0.038			
					54834.4817	19.932	0.103			
56	9.0	12.8,18.8	0.130	0.100	54858.8590	20.047	0.088	53730.1469	23.925	—
					55209.2057	20.082	0.035			
					53419.5906	20.071	0.035			
					53756.3509	20.106	0.030			
57	12.8	16.0,22.0	0.090	0.090	53758.3800	20.210	0.046	53924.0757	22.060	—
					53766.7386	20.113	0.042			
					53781.7254	19.785	0.126			
58	12.8	16.0,22.0	0.090	0.090	54493.4773	19.776	0.125	53731.1542	23.828	—
					53400.5816	20.375	0.172			
					53419.5906	20.069	0.040			
					53756.3500	20.126	0.033			
					53758.3799	20.310	0.057			
					53766.7385	20.216	0.052			
					54834.4817	20.310	0.155			
59	12.8	16.0,22.0	0.090	0.090	54858.8592	20.142	0.110	53757.9418	23.404	0.414
					55209.2056	20.100	0.041			
					53400.5753	20.128	0.134			
					53419.5907	20.109	0.041			
					53756.3530	20.176	0.034			
					53758.3799	20.189	0.051			
					53766.7385	20.128	0.046			
					54834.4817	20.135	0.128			
					54858.8591	20.279	0.110			
					55209.2055	20.165	0.042			

**Table 3** *continued on next page*

**Table 3** (*continued*)

ID	Ap. Rad. (")	Annulus Rad. (")	NUV Ap. Corr. (mag)	FUV Ap. Corr. (mag)	NUV Epoch (MJD)	NUV Mag.	NUV Mag. Error	FUV Epoch (MJD)	FUV Mag.	FUV Mag. Error
60	12.8	16.0,22.0	0.090	0.090	53419.5907	20.163	0.045	53717.0241	22.933	0.310
					53756.3530	20.113	0.033			
					53758.3799	20.079	0.048			
					53766.7386	20.249	0.055			
					53781.7254	20.222	0.213			
					54493.4772	20.498	0.247			
61	12.8	16.0,22.0	0.090	0.090	53400.5783	20.085	0.124	53729.1541	23.609	0.564
					53419.5907	20.314	0.049			
					53756.3534	20.197	0.035			
					53758.3800	20.141	0.046			
					53766.7386	20.150	0.049			
					54834.4818	20.466	0.174			
					54858.8590	20.210	0.109			
62	12.8	16.0,22.0	0.090	0.090	55209.2055	20.257	0.045	53738.8087	23.547	0.516
					53400.5815	20.047	0.124			
					53419.5909	20.238	0.045			
					53756.3519	20.323	0.038			
					53758.3799	20.436	0.063			
					53766.7386	20.424	0.060			
					54834.4817	20.308	0.154			
63	12.8	16.0,22.0	0.090	0.090	54858.8591	20.448	0.134	53709.9918	23.721	—
					55209.2059	20.138	0.040			
					53419.5908	20.277	0.050			
					53756.3488	20.354	0.041			
64	12.8	16.0,22.0	0.090	0.090	53758.3800	20.351	0.062	53723.9751	23.811	—
					53766.7388	20.396	0.065			
					53400.5784	20.184	0.141			
					53419.5905	20.240	0.045			
					53756.3509	20.327	0.037			
					53758.3797	20.279	0.054			
					53766.7386	20.305	0.054			
					54834.4817	20.447	0.172			
					54858.8590	20.156	0.103			
					55209.2055	20.228	0.044			

**Table 3** *continued on next page*

**Table 3** (*continued*)

ID	Ap. Rad. (")	Annulus Rad. (")	NUV Ap. Corr. (mag)	FUV Ap. Corr. (mag)	NUV Epoch (MJD)	NUV Mag.	NUV Mag. Error	FUV Epoch (MJD)	FUV Mag.	FUV Mag. Error
65	12.8	16.0,22.0	0.090	0.090	53400.5850	20.405	0.170	53776.6713	23.569	—
					53419.5906	20.239	0.045			
					53756.3496	20.308	0.038			
					53758.3799	20.372	0.060			
					53766.7385	20.387	0.059			
					54834.4817	20.285	0.154			
					54858.8591	20.317	0.123			
66	9.0	12.8,18.8	0.130	0.100	55209.2054	20.243	0.045	53683.3276	24.099	—
					53419.5909	20.514	0.049			
					53756.3514	20.465	0.037			
					53758.3800	20.628	0.062			
					53766.7386	20.559	0.057			

NOTE—ID is the source identification number given in Table 1. Ap. Rad. is the aperture radius used to extract photometry for both bands. Annulus Rad. is the inner, outer radii respectively used to define the background annulus region. NUV and FUV Ap. Corr. are the aperture corrections for each band; to apply these corrections, subtract them from the reported photometry in the table. NUV Epoch is the Modified Julian Date of the photometric value reported for each row. NUV Mag. and Mag. Error are the extracted AB magnitude and associated uncertainty respectively for the corresponding epoch. FUV Epoch reports the average Modified Julian Date for each source after integrating all available FUV data. FUV Mag. is the corresponding extracted AB magnitude. FUV Mag. Error reports the uncertainty when a source detection is made (see Section 3), otherwise a “—” indicates the FUV Mag. is an upper limit.